JOURNAL OF GEOPHYSICAL RESEARCH, VOL. 102, NO. D25, PAGES 29,991-30,002, DECEMBER 27, 1997

Comparison of model estimated and measured direct-normal solar irradiance

Rangasayi N. Halthore,[1] Stephen E. Schwartz,[1] Joseph J. Michalsky,[2]
Gail P. Anderson,[3] Richard A. Ferrare,[4] Brent N. Holben,[5]
and Harry M. Ten Brink,[6]

Abstract. Direct-normal solar irradiance (DNSI), the energy in the solar spectrum incident in unit time at the Earth's surface on a unit area perpendicular to the direction to the Sun, depends only on atmospheric extinction of solar energy without regard to the details of the extinction, whether absorption or scattering. Here we report a set of closure experiments performed in north central Oklahoma in April 1996 under cloud-free conditions, wherein measured atmospheric composition and aerosol optical thickness are input to a radiative transfer model, MODTRAN 3, to estimate DNSI, which is then compared with measured values obtained with normal incidence pyrheliometers and absolute cavity radiometers. Uncertainty in aerosol optical thickness (AOT) dominates the uncertainty in DNSI calculation. AOT measured by an independently calibrated Sun photometer and a rotating shadow-band radiometer agree to within the uncertainties of each measurement. For 36 independent comparisons the agreement between measured and model-estimated values of DNSI falls within the combined uncertainties in the measurement (0.3-0.7%) and model calculation (1.8%), albeit with a slight average model underestimate (-0.18 ± 0.94)%; for a DNSI of 839 W m^{-2} this corresponds to -1.5 ± 7.9 W m^{-2}. The agreement is nearly independent of air mass and water-vapor path abundance. These results thus establish the accuracy of the current knowledge of the solar spectrum, its integrated power, and the atmospheric extinction as a function of wavelength as represented in MODTRAN 3. An important consequence is that atmospheric absorption of short-wave energy is accurately parametrized in the model to within the above uncertainties.

1. Introduction

One of the main goals of the present generation atmospheric radiation studies is to perform closure experiments wherein model estimates are compared to measurements of atmospheric radiation components [*Penner et al.*, 1994; *Stokes and Schwartz*, 1994; *Quinn et al.*, 1996]. Such model evaluation can lead to important consequences for global weather and climate prediction by better constraining global atmospheric models. Here we perform a simple yet robust closure experiment. We examine the ability of a moderate resolution radiative transfer model to accurately estimate direct-normal solar irradiance (DNSI). This is the energy in the solar spectrum falling per unit time on a unit area of a surface oriented normal to the Sun's direction from a narrow solid angle that encompasses the Sun. The units of DNSI are watts per square meter. DNSI is a simple quantity because it depends only on the amount of energy incident at the top of the atmosphere and the extinction properties of the constituents of the atmosphere without regard to details of extinction, such as scattering versus absorption or the angular distribution of scattered light. We choose only clear days to avoid complications arising from the presence of clouds. By clear we mean that the sky around the Sun's disk is free of visible clouds which may, however, be present elsewhere in the sky. This experiment tests (1) the knowledge of the energy in the extraterrestrial Solar spectrum and its spectral distribution; (2) the ability to measure or calculate attenuation due to atmospheric constituents, including major atmospheric constituent gases (Rayleigh scattering), trace gas species (absorption), and aerosols (scattering and absorption); and (3) the accuracy with which the irradiance is measured. The magnitude of the systematic and random departure between model-estimated and measured DNSI is thus a measure of the combined uncertainties in the measurements and in the description of solar spectrum and attenuation represented in the model. If the model estimated and measured DNSI agree for a large number of cases, then it must be concluded, in the absence of fortuitous circumstances where one effect mitigates another, that the major items affecting atmospheric attenuation listed above are well understood and accurately measured. If they do not agree, the study performed here will aid in identifying the cause of the disagreement and in determining the sensitivity of the disagreement to the propagated uncertainty of the above quantities.

The current work was motivated in part by recent studies examining atmospheric absorption of short-wave energy

[1]Department of Applied Science, Brookhaven National Laboratory, Upton, New York.
[2]Atmospheric Sciences Research Center, State University of New York at Albany.
[3]Phillips Laboratory/Geophysics Directorate, Hanscom Air Force Base, Massachusetts.
[4]Hughes STX Corporation, Lanham, Maryland.
[5]NASA Goddard Space Flight Center, Greenbelt, Maryland.
[6]Netherlands Energy Research Foundation, ECN, Petten, Netherlands.

Paper number 97JD02628.
0148-0227/97/97JD-02628$09.00

[*Cess et al.*, 1995; *Li et al.*, 1995; *Pilewskie and Valero*, 1995; *Ramanathan et al.*, 1995; *Wiscombe*, 1995; *Arking*, 1996; *Imre et al.*, 1996, *Stephens*, 1996] and the resultant need to identify possible causes for apparent absorption in excess of that represented by current models. Even cloudy atmospheres, the subject on which much of the recent attention has been focused, consist in large part of clear (cloud free) air, and it is thus useful to examine the accuracy with which current models represent short-wave transmission in clear air to determine possible causes of apparent excess absorption. Inadequate description of clear-sky absorption might be manifested as error in describing absorption in the cloudy column, because of increased effective photon path length resulting from multiple scattering in the column. Thus it is necessary to examine the accuracy of current knowledge of band and continuum absorption of gases, including water vapor, as represented in models of atmospheric transmittance.

This study uses measurements made at the Department of Energy's (DOE) atmospheric radiation measurement (ARM) cloud and radiation test bed (CART) site Central Facility (CF) in north central Oklahoma during an intensive observational period (IOP) in April 1996. We use instantaneous values of Sun photometer-measured aerosol optical thickness (AOT) at discrete wavelengths in the visible and near-IR, and radiosonde-measured temperature and humidity as a function of pressure (and hence altitude) as input to a moderate resolution (2 cm^{-1}) radiative transfer model (MODTRAN 3, version 1.3, identical to MODTRAN 3.5 for DNSI calculation) [*Anderson et al.*, 1995] to estimate DNSI. (Here and throughout the paper we use the term aerosol optical thickness (AOT, or τ_a) to denote the vertical (air mass = 1) aerosol optical thickness). The performance of MODTRAN 3 is evaluated against a line-by-line radiative transfer code that uses a comprehensive and current version of the molecular database. The sensitivity of the estimated DNSI to errors and uncertainties in the input parameters is examined. The calculated DNSI is then compared with values measured by using two well-calibrated absolute cavity radiometers (ACRs) and two normal incidence pyrheliometers (NIPs), themselves calibrated by intercomparison with the ACRs.

2. Background

Any model that estimates DNSI, E, needs as input the extraterrestrial spectral solar irradiance (referred to the mean Sun-Earth distance) $E_0(\lambda)$, in addition to the quantities that are needed to compute the spectral transmittance of the atmosphere $T(\lambda,\mu_0)$, as a function of wavelength λ along the slant path to the top of the atmosphere that corresponds to solar zenith angle θ_0 ($\mu_0 = \cos\theta_0$) at the time of measurement. Thus

$$E = \left(\frac{1}{R^2}\right)\int E_0(\lambda)T(\lambda,\mu_0)d\lambda \ , \qquad (1)$$

where integration is performed over the solar spectrum, R is the Sun-Earth distance at the time of measurement in astronomical units (AU) (mean Sun-Earth distance = 1 AU), and the transmittance T(λ) is given by Bouguer's law,

$$T(\lambda,\mu_0) = T_{\text{Rayleigh}}(\lambda,\mu_0)T_{\text{gas}}(\lambda,\mu_0)T_{\text{acrosol}}(\lambda,\mu_0),$$

$$= \exp-\{(m\tau^{\lambda})_{\text{Rayleigh}} + (m\tau^{\lambda})_{\text{gas}} + (m\tau^{\lambda})_{\text{acrosol}}\}, \qquad (2)$$

where m is the component air mass along slant path, defined in the absence of refractive effects as $m = 1/\mu_0 = 1/\cos\theta_0$, and each τ_i denotes a contribution to vertical optical thickness due to the indicated atmospheric component. The three major components that cause attenuation of solar energy are Rayleigh or molecular scattering, gaseous absorption due to ozone, oxygen, water vapor, nitrogen (continuum), carbon dioxide and other gases, and absorption and scattering by aerosols. The error in the calculated DNSI arises from the error in the solar spectrum as represented in the model and the error in the estimate of the atmospheric transmittance, under the assumption that the Sun-Earth distance and the air mass are accurately known.

Data available from the National Geophysical Data Center, Boulder, Colorado, show that the extraterrestrial total solar irradiance as measured by a number of Earth-orbiting satellites (SMM, ERBS, NOAA 9, NOAA 10, and UARS) is 1366 ±3 W m^{-2} for observations over the last 15 years [*Lean*, 1991]. The uncertainty includes bias among different sensors and is due mainly to differences in calibration. Data from any one sensor show long-term (11 years) periodicity (sunspot cycle) whose amplitude is about 1.3 W m^{-2}. In contrast to the total solar output, the spectral solar output is not that well known and is, furthermore, variable. Most radiative transfer models use the *Neckel and Labs* [1984] data are shown to disagree with other data sets to 1% in the visible and near IR and to 5% in the mid IR [*Markham and Barker*, 1987]. It is not clear what effect this uncertainty has on the evaluation of DNSI, especially when the solar spectrum is convolved with the individual gaseous absorption coefficients to obtain DNSI.

For an atmosphere that is free of water vapor and aerosols, two of the most variable components of the atmosphere, a simulation with MODTRAN 3 shows that for a solar zenith angle of 60° the effective attenuators of solar energy in the 0.2 to 5 μm region in decreasing order of importance are Rayleigh scattering (attenuation ≈ 15%), ozone (3.5%), carbon dioxide (1.2%), oxygen (0.8%), methane (0.3%), nitrogen continuum (0.13%), nitrogen dioxide (0.12%), nitrous oxide (0.11%), sulfur dioxide (0.1%), and carbon monoxide (0.01%). Attenuation due to Rayleigh scattering is accurately estimated by models, including MODTRAN 3, because it depends mainly on the surface pressure, which is well known, and is only a weak function of the type of atmosphere present (i.e., the atmospheric lapse rate). For the minor gases the attenuation is due entirely to absorption. Here the "standard" or "default" amounts of attenuating gases available in the program were used. Except for Rayleigh scattering and absorption by ozone and water vapor, uncertainty in the abundance of gases leads to negligible (<1 W m^{-2}) changes in DNSI. For example, increasing carbon dioxide mixing ratio from 330 to 350 ppm changes DNSI by 0.1 W m^{-2}. Uncertainty in ozone column abundance, which might arise from using a climatological value instead of actually measuring the instantaneous value by ozonesondes or by satellite retrievals, has a slightly larger effect on the DNSI. For example, as discussed below, a 20% error in the estimate of ozone column abundance leads to an error in the DNSI estimate of 0.6% (4 W m^{-2} at 650 W m^{-2}). This is about the same magnitude as an error of 10% in water column abundance. Thus it is necessary to check climatological ozone column abundance against actual

measurements for each simulation. In what follows we discuss MODTRAN 3 inputs and their sensitivity to DNSI prediction to illustrate the most important quantities that need to be measured accurately for a good closure. It will be shown that the calculated DNSI exhibits the greatest sensitivity to the most variable components of the atmosphere, aerosols and water vapor, and hence that it is these quantities that need to be most accurately characterized.

3. MODTRAN 3 Evaluation and Sensitivity to Inputs

MODTRAN 3 was developed to perform moderate resolution (2 cm^{-1}) radiative transfer computations in the Earth's atmosphere. It uses a high-resolution solar spectrum derived from the work of *Kurucz* [1995] and, with some exceptions, is consistent with the data of *Neckel and Labs* [1984]. The total integrated extraterrestrial output used in MODTRAN 3 is 1373.2 W m^{-2}, which is at the upper limit of the measurements indicated above. In the direct solar irradiance mode, the model computes DNSI at the surface, whose altitude can be specified. The transmission is computed by including contribution from all attenuators, molecular scattering, gaseous absorption, and aerosol attenuation. Atmospheric lapse rate (pressure and temperature as a function of altitude in the atmosphere) and water column abundance (relative humidity) are specified, for example, from radiosonde values. Aerosol extinction, single-scattering albedo, and asymmetry parameter are specified at discrete wavelengths throughout the short wave. Extinction, in the model, is defined as the ratio of AOT at a given wavelength to that at 550 nm. The wavelengths at which AOT is required for model input does not coincide with those at which it is measured; hence interpolation or extrapolation is required, using the Ångström power law, $\tau_a \propto a\lambda^{-b}$, where a and b are constants and b is the Ångström exponent. Although MODTRAN 3 allows specification of single scattering albedo and asymmetry parameter, their correct specification, even if practical, is not necessary for this closure experiment. Ozone column abundance is chosen from among the "standard" atmospheres (five are available in the model) to agree with measured values.

MODTRAN 3 uses band models based on the HITRAN 96 (*L. S. Rothman et al.*, manuscript in preparation, 1997) line listing and thus reflects the current knowledge of the physics of transmission of the atmospheric molecular constituents. MODTRAN 3 prediction of direct-normal spectral solar irradiance (DNSSI), defined as the DNSI in specific absorption bands and in this context the atmospheric absorption bands of H_2O, O_2, and CO_2, is evaluated by comparing with the DNSSI calculation of FASE (FASCODE for Environment) [*Snell et al.*, 1997], a line-by-line code, based on a line-by-line radiative transfer model (LBLRTM), [*Clough*, 1992], which is used in conjunction with the HITRAN 96 database. This comparison of the two models for the same atmosphere and geometry is performed to test the adequacy of band model parameterizations in MODTRAN 3. The comparison (Table 1) shows that the percentage difference, shown in column 6, is within 0.6% in all of the molecular bands. The impact of the observed difference in any one band on the DNSI integrated over the entire solar spectrum is negligible. For example a 0.6% error in the estimate of the DNSSI in the H_2O band in the range 8400-9400 cm^{-1} leads to an error of 0.3 W m^{-2} (or 0.03% in a measurement of 800 W m^{-2}) in DNSI. The combined effect of error in all the bands has an impact on the DNSI of about 0.3%, as seen in the last row of Table 1. Thus the band model parameterizations of the important molecular absorption bands are adequate and lead to an estimate of DNSI that is consistent with an estimate of a more accurate line-by-line radiative transfer code. Ozone bands are not included in this table since they are handled as identical Chappuis continua [*Shettle and Anderson*, 1995] in both FASE and MODTRAN 3.

The sensitivity of DNSI to atmospheric variables AOT, precipitable water (PW), Ångström exponent, ozone column abundance, and a combination of AOT and PW is examined in Table 2. A base case in row 1 is identified as $\tau_a(550)$ of 0.095, PW of 1.087 cm, Ångström exponent of 0.6, CO_2 abundance of 330 ppm, and ozone vertical column abundance of 324 DU (1 Dobson unit = 1 m atm cm = 2.69×10^{16} molecules cm^{-2}). Except for CO_2 and ozone these values

Table 1. Comparison Between DNSI Predicted by MODTRAN 3 and FASE in Specific Wavelength Bands Corresponding to Molecular Absorption

Molecule	Wave number Range, cm^{-1}	Wavelength Range, mm	FASE, W m^{-2}	MODTRAN, W m^{-2}	Percent Difference
CO_2	2000-3000	3.3-5.0	7.99	7.946	0.58
H_2O	5000-5600	1.6-2.0	4.09	4.069	0.55
H_2O	7000-7390	1.35-1.43	0.349	0.3492	0.15
H_2O	8400-9400	1.06-1.19	49.4	49.08	0.64
H_2O	10580-10695	0.935-0.945	3.57	3.558	0.41
H_2O	11500-12600	0.794-0.869	67.2	67.2	-0.08
O_2	12800-13170	0.759-0.781	20.9	20.58	0.48
O_2	14310-14560	0.687-0.699	14.7	14.5	0.16
H_2O	15000-15800	0.633-0.667	47.9	47.9	0.06
O_2	15710-15930	0.628-0.637	12.8	12.7	0.07
All	2000-50,000	0.2-5 mm	998	995.0	0.3

U.S. Standard Atmosphere is used for a solar zenith angle of 45° for both model runs.

Table 2. Sensitivity of Direct-Normal Solar Irradiance to the Input Parameters

Item	AOT 550	Precipitable Water, cm	Ångström Exponent	Ozone Column Abundance, DU	Predicted Irradiance, W m^{-2}	Difference From Base Case, W m^{-2}
Base case	0.095	1.087	0.6	324	805.9	
AOT	0.085	1.087	0.6	324	819.4	13.5
PW	0.095	1.196	0.6	324	801.8	-4.1
Ångström Exponent	0.095	1.087	0.5	324	802.9	-3.0
Ozone	0.095	1.087	0.6	400	802.6	-3.3
AOT & PW	0.085	1.196	0.6	324	815.3	9.4

Calculations were performed for the CART site in Oklahoma, 36° 36' N, 97° 24' W, 315 m above sea level, for data obtained on April 18, 1996, at 1427 UTC, when the solar zenith angle was 59.7°.

were measured at the CART site on April 18, 1996, at 1427 UT when the solar zenith angle was 59.7°. The computed DNSI is 805.9 W m^{-2}. The subsequent rows in the table show the effect of changing the value of one or more atmospheric variables by an amount roughly corresponding to its uncertainty. Decreasing AOT at 550 nm by 0.01 (this value reflects current state of the art accuracy in AOT measurements, as discussed below) increases the predicted DNSI by 13.5 W m^{-2}. Increasing PW by 10%, the uncertainty of radiosonde measurement (as deduced by comparing against other independent methods, including those using Sun photometers and microwave radiometers, here as well as elsewhere [*Halthore et al.*, 1997, *Lesht and Liljegren*, 1997] decreases the DNSI by only 4.1 W m^{-2}. Increasing the ozone column abundance by 28%, close to the typical uncertainty of 20% obtained if one uses climatological values, decreases DNSI by 3.3 W m^{-2}. Decreasing the Ångström exponent from 0.6 to 0.5, a fairly substantial change, decreases DNSI by 3 W m^{-2}. A combination of changes in the above quantities, for example PW and AOT, yields a change in DNSI that is roughly equal to the sum of the changes taken separately, 9.4 W m^{-2}. Thus uncertainty in AOT has the most influence. The reason for this is that aerosol attenuation is present in the entire solar spectrum as opposed to discrete absorption in the molecular absorption bands. Therefore it is important that AOT be accurately specified as input to MODTRAN 3; measurement of this quantity at the CART site is discussed next. The percent uncertainty in the estimate of DNSI, using MODTRAN 3 due to AOT, PW, Ångström exponent, and ozone column abundance, is thus estimated to be 1.8%, where the uncertainties are summed by assuming that they are uncorrelated.

4. Measurement of Model Inputs and Uncertainty

4.1. Aerosol Optical Thickness

Determination of AOT from DNSSI measurements at the surface is a well-known procedure, and extensive literature on the subject exists [*Shaw*, 1983; *Bruegge et al.*, 1992; *Harrison et al.*, 1994]. At the CART site, the measurement of DNSSI is accomplished by two types of instruments: narrow field-of-view (1.2°) Sun photometer, which measures direct irradiance in several spectral bands, and horizontally placed shadow-band radiometers which measure the hemispherical downward total and diffuse-sky irradiance, again in several spectral bands. In the latter case, the direct irradiance is obtained by the difference of total and diffuse spectral irradiance divided by the cosine of the solar zenith angle. Thus the two types of instruments measure components of the total hemispherical-downward irradiance at the surface.

The Sun photometer (Cimel Electronique, Paris, France; hereinafter called the Cimel Sun photometer), having a field of view of 1.2°, measures AOT in seven different bands of ~10 nm bandwidth throughout the visible and near-IR [*Holben et al.*, 1997]. A 940-nm band (also 10 nm bandwidth), centered on a water absorption band, is used to measure the water column abundance [*Halthore et al.*, 1997]. It takes three measurements spaced 30 seconds apart in all the channels to aid in the discrimination against clouds. If the path to the Sun is determined to be clear, the three measurements are averaged to obtain AOT and PW. Calibration is performed at a mountain site by the Langley plot method for the AOT channels [*Shaw*, 1983; *Halthore et al.*, 1992a] and by the Modified Langley Method for the water vapor channel [*Reagan et al.*, 1987]. Both these methods of calibration obtain the necessary calibration coefficients without the need to measure irradiance; the transmittance of the atmosphere is inferred directly. Thus DNSI determination from measurements of atmospheric transmittance at discrete wavelengths throughout the short-wave spectrum leads to an independent closure experiment. The estimated uncertainty in AOT determination for the Cimel Sun photometer is ±0.01 at an air mass of 1; this is the accuracy of calibration at Mauna Loa, Hawaii, generally considered to be the world's best site for such calibrations because of the low and stable AOT due to its location far from continental sources and altitude well above the marine boundary layer during mornings. The Cimel Sun photometer calibration coefficients were obtained as an interpolation between those obtained at Mauna Loa and the subsequent intercomparison with an instrument that was calibrated at Mauna Loa. For the water vapor column abundance determination the uncertainty is about ±10%, which is the same as that for a radiosonde measurement.

A multifilter rotating shadow-band radiometer (MFRSR) (Yankee Environmental Systems, Inc., Turners Falls, Massachusetts) [*Harrison et al.*, 1994] measures AOT in six bands in the visible and near IR, some of which are

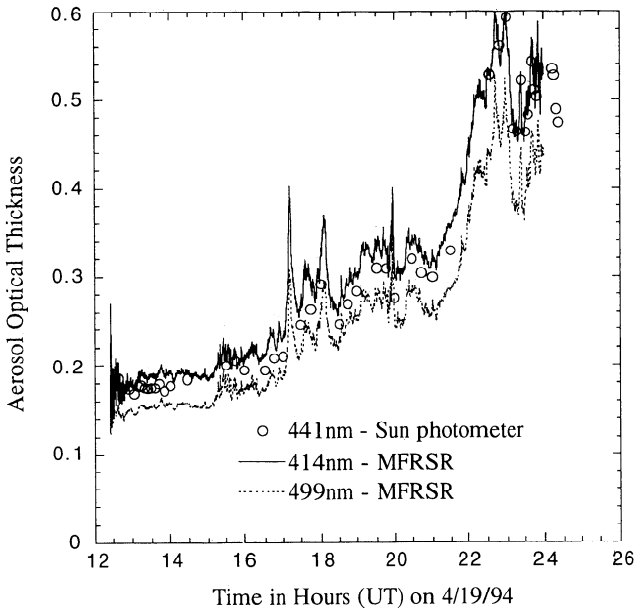

Figure 1. Comparison of MFRSR measured AOT in two channels (414 and 499 nm) with that measured using Cimel Sun photometer in 441 nm channel for April 19, 1994, CART ARM site in Oklahoma. Local standard time is 0600 UT.

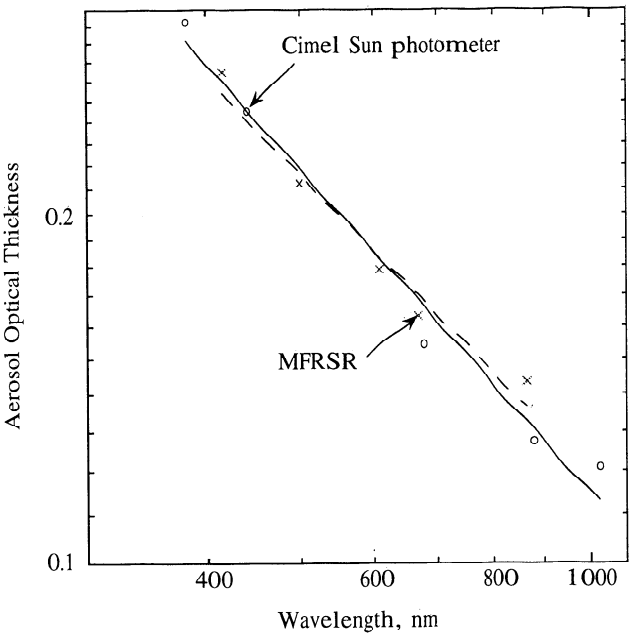

Figure 2. Ångström fits to AOT curve obtained by Cimel Sun photometer (circles, solid line) and MFRSR (crosses, dashed line) at the CART ARM site in Oklahoma on April 19, 1994, at 1730 UT. Ångström exponents are 0.921 and 0.848, respectively. This figure shows that the two instruments yielded the same AOT as a function of wavelength despite their completely independent methods of calibration.

coincident in center wavelength with those of Cimel Sun photometer. It also has a 940 nm channel for water column abundance determination. The effective field of view, governed by the width of the shadow band, is slightly larger than the umbral angle of 3.27°. The MFRSR is also calibrated by the Langley plot method and modified langley method [*Michalsky et al.*, 1995] but at the CART site itself. In both 1994 and 1996, for the data shown here, the MFRSR was calibrated by obtaining Langley plots on selected days when the AOT was generally low and, more importantly, stable. The resultant accuracy of AOT determination is ±0.02 (double that for Cimel Sun photometer calibrated at Mauna Loa) and ±10% for the water column abundance determination (as for the Cimel Sun photometer). The higher uncertainty in AOT determination arises from relatively poor air quality of the CART site for calibration, when compared to that at Mauna Loa, due to the higher and more variable AOT.

A comparison between MFRSR and Cimel-Sun-photometer-derived AOT, over the course of a single day, is shown in Figure 1. The measurements from the two channels on the MFRSR (414 and 499 nm) bracket those from the 441 nm channel on the Cimel Sun photometer, with all three comparably following the increasing trend over the course of the day. The closeness of the agreement in AOT in the several wavelength channels is seen in an Ångström plot (log AOT versus log wavelength) (Figure 2). The two instruments yielded virtually the same magnitude and wavelength dependence of AOT despite their completely independent calibrations. These data are typical of those obtained in April 1994. Thus we conclude that the AOT measured by Cimel and MFRSR in April 1994 at the ARM CART site are in agreement to within ±0.01.

Another example of such a comparison, from April 1996 (Figure 3), again shows agreement of AOT values derived from the MFRSR and the Cimel Sun photometer to within the accuracy of the measurements (at an air mass of 1) of 0.02 and 0.01, respectively. Agreement is excellent (<0.005) in the late evening but not in the morning or afternoon. The disagreement is still however, within the accuracy of the measurements using the two instruments. Systematic

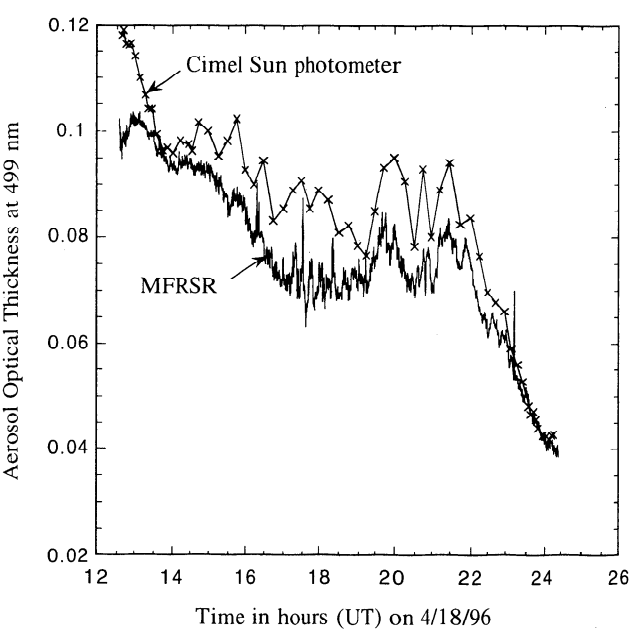

Figure 3. Comparison between AOT at 499 nm derived from MFRSR and Cimel Sun photometer (crosses) located next to each other at the CART ARM site in Oklahoma on April 18, 1996. Local standard time is 0600 UT.

departures are observed which cannot be explained by simply a change of the calibration coefficient. The systematic difference observed in Figure 3 between the two instruments is assumed to result from the misleveling of the sensor head in the MFRSR, although lack of temperature control of the detector and filters in the Cimel Sun photometer could be another source. We use only the Cimel Sun-photometer-derived AOT, as its uncertainty (0.01) is smaller than the estimated uncertainty of MFRSR measurements (0.02).

4.2. Precipitable Water and Ozone Column Abundance

Two independent measurements of PW (one from the in situ radiosonde measurements as a function of height and the other from the column-integrated Cimel Sun photometer measurement in the 940 nm band) are compared in Figure 4 and Table 3. Since the period in April, of interest here, was part of an intensive observations period (IOP) of ARM, radiosondes were launched every three hours. Figure 4 shows a comparison of precipitable water derived by Sun photometer and radiosonde measurements. For 10 out of 13 cases (a subset of the total number of cases which correspond to the time of radiosonde launch) the numbers are within ±10% of radiosonde values. Radiosonde measurements of precipitable water vapor agree to within ±10% of microwave radiometer measurements made at the SGP/CART site during April 1996. Some of the variability may be related to differences between radiosonde calibration lots [*Lesht and Liljegren*, 1997] but also may result from horizontal nonuniformity in the distribution of water vapor. Thus the Sun photometer and radiosonde measurements are consistent to within the expected uncertainty in the PW measurement of ±10%. Also listed in Table 3 are ozone column abundance as measured by TOVS (TIROS N operational vertical sounder). The TOVS data extracted for the location of the CART site at 1800 UT for each day [*Neuendorffer*, 1996] have an uncertainty of ±25 DU (~±8%). In all the model runs reported in this paper we have used ozone values corresponding to standard midlatitude summer profile which is close to 325 DU. Thus the TOVS values are within 20% of the assumed values from climatology yielding no more than ±3 W m^{-2} uncertainty in the computed DNSI (Table 2).

Table 3. PW and Ozone Column Abundance for Each Day for Which the Closure Experiment is Performed

Date	Time, UTC	PW Sun Photometer, cm	PW Radiosonde, cm	Ozone Column Abundance TOVS (1800 UTC), DU
4/13/96	1434:05	0.981	1.12	
4/13/96	1730:28	1.106	1.18	342
4/15/96	1459:55	0.825	0.77	
4/15/96	1729:57	0.901	0.85	374
4/15/96	2014:56	0.895	0.75	
4/18/96	1427:30	1.0046	1.087	
4/18/96	1729:16	0.7199	0.66	313
4/18/96	2029:14	0.7209	0.728	
4/19/96	1729:03	1.086	1.11	310
4/19/96	2325:24	0.85	0.92	
4/20/96	1431:35	0.823	0.862	350
4/23/96	1428:14	0.934	0.913	
4/23/96	1728:14	1.0306	1.14	366

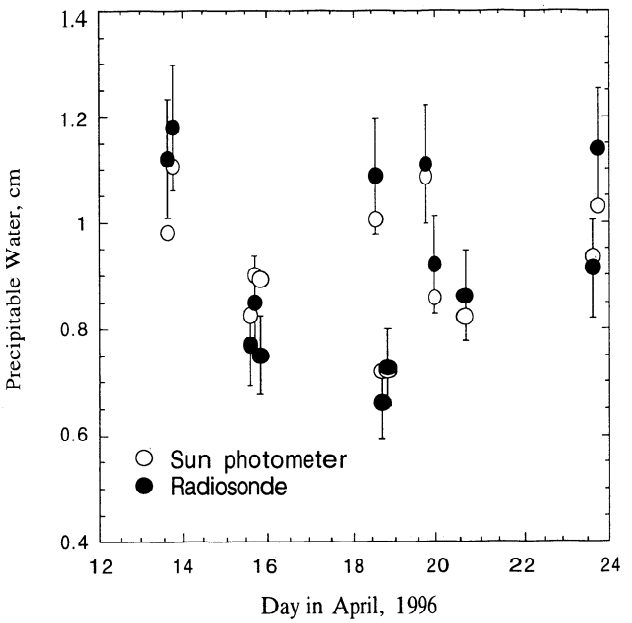

Figure 4. Precipitable water as obtained by Sun photometer and radiosonde are plotted against date in April 1996, in UT; local standard time (in days) is 0025 UT. The error bars on the radiosonde values denote the expected uncertainty of radiosonde measurements of PW of ±10%. For 10 cases of the 13, the two methods agree to within ±10%.

4.3. Corrections to MODTRAN 3 Estimates of DNSI

Since MODTRAN 3 uses solar spectrum from the Kurucz model (discussed above) which is consistent with Neckel and Labs data, the solar constant, obtained by integrating over the solar spectrum, is 1373.2 W m^{-2}, slightly greater than the generally accepted value based on satellite observations of 1366 ±3 W m^{-2} [*Lean*, 1991] (see section 2). Model estimates are therefore decreased by 0.52% to account for the use of slightly higher solar constant.

Calculation with MODTRAN 3 are made for the wavelength range 0.2-5 μm to limit the number of calculations required beyond 5 μm. However, the absolute cavity radiometer, and after calibration with the ACR, the NIP, are sensitive to the entire solar spectrum. The energy in the extraterrestrial solar spectrum beyond 5 μm is 0.45% of the total energy (from the solar spectrum used in MODTRAN 3); however, at the surface, model calculation shows that energy beyond 5 μm is only 0.11% of the total. Thus the model calculated value is increased by 0.11% .

4.4. DNSI Measurement and Its Uncertainty

DNSI data as measured by two ACRs and two NIPs are used here. The ACRs are Eppley model AHFs that measure DNSI with a 5° field of view by comparing the heating of a cavity that is irradiated by the direct solar beam with the heating by an electrical circuit. These types of cavity radiometers are also called "electrical substitution cavity radiometers." The two ACRs were used at the CART site on April 18, 19, 20, and

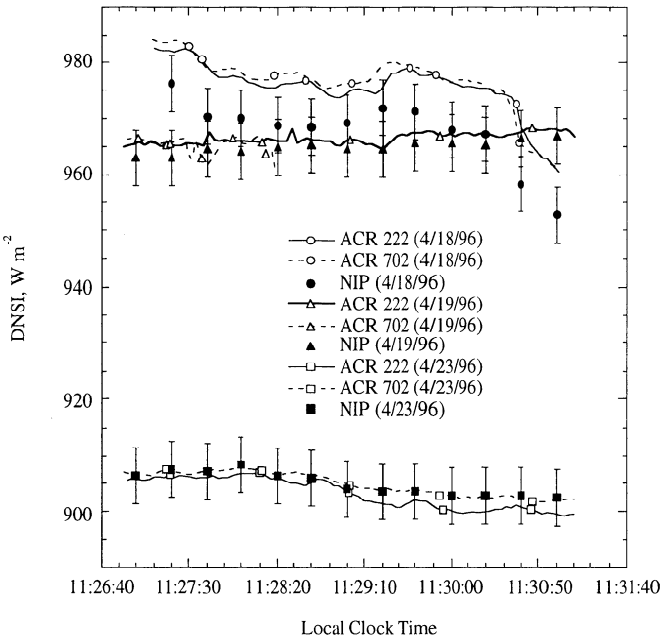

Figure 5. DNSI as measured by the two ACRs and the NIP are shown for identical periods (~4 min) for three different days, April 18, 19, and 23, during which period a closure experiment is performed. The NIP values are made to agree with ACR values on April 23. See text on reasons why the agreement on April 19 is excellent while that on April 18 is not so good. For days before and including April 18, recalibration of NIP values was done. The error bars on NIP values represent ±5 W m^{-2}.

23 (M. Rubes and J. DeLuisi, private communication, 1996) during most of the day when the sky was cloud free in the Sun's direction. During this period the two ACRs agreed to within 2 W m^{-2} (Figure 5) except during the early part of April 18 (not shown) when one of the ACRs showed relatively large fluctuations in its output. The ACRs provide a measurement every 3 s. The calibration accuracy of the ACRs can be traced to World Radiation Reference (WRR) Standards in October 1995 that is stated to be 0.3% or better [*Romero et al.*, 1995/1996]. In Figure 5, DNSI measured by the two ACRs for identical periods lasting about 4 minutes on three days, April 18, 19, and 23, is shown. Validation of the 0.3% accuracy in calibration is clearly seen in this figure by the closeness of the ACR curves on all three days.

Figure 5 also shows the results of measurements by an Eppley model normal incidence pyrheliometer (NIP) which is used with a suite of radiometric instruments at the surface on the SIROS (Solar and Infrared Observation Station) platform. The NIP works by radiant heating of the hot junction of a thermopile sensor and has a 5.7° field of view. It provides an instantaneous measurement of DNSI every 20 s. NIP data are available continuously for long periods of time because it is a facility instrument. The SIROS NIP is calibrated by comparison with the ACRs on April 23. This calibration showed that a previous calibration used to report DNSI values in the database was underestimating the DNSI by 2.1% [*Michalsky et al.*, 1997]. Using the April 23 calibration constant, the excellent agreement (well within 3 W m^{-2} in Figure 5) seen on April 19 between the NIP and the ACR is indicative of the stability of the NIP. On the morning of April 19, a jump in the response of the NIP is seen which is due to cleaning of the glass window. Thus the calibration factor, deduced from April 23 and applicable to periods after the April 19 morning, is seen to underestimate the DNSI on April 18 by about 0.9%. For dates before April 19, the SIROS NIP was recalibrated with the use of ACR data obtained on April 18. Once calibrated, the NIP tracked the DNSI to within about 3 W m^{-2} of the ACR values, when the latter were available. An almost identical NIP that is part of the Baseline Radiation Network (BSRN) was taking measurements of DNSI nearby, at 1 s interval, during April 13-23. The data from this instrument helped establish the stability of the SIROS NIP during days in which ACR data were not available (April 13 and 15). Figure 6 shows for a 12 min interval during a day that encompasses the interval shown in Figure 5, a comparison of DNSI measured by the two NIPs, both of which were calibrated by comparison with ACRs on April 18. The data are degraded to a resolution of 80 s. It appears that the glass window on the BSRN NIP was also cleaned at the same time on the April 19 morning when a jump in the NIP response was seen in the DNSI trace (not shown). The ratio of calibration coefficients for the two NIPs on April 19 and 23 before and after cleaning is identical. Once calibrated, two NIPs tracked to within 0.6% (5 W m^{-2} at 800 W m^{-2}) on all days used in this study, thus establishing the stability of both the instruments. Thus the uncertainty in DNSI measurement using either NIP is an appropriate sum of the uncertainty in the ACR measurement of 0.3% and the uncertainty in the stability of the NIP response, assumed here

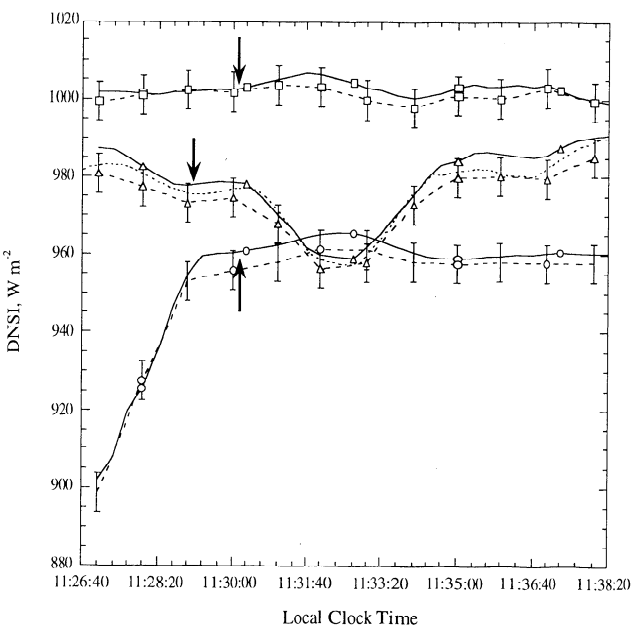

Figure 6. DNSI as measured by the two NIPs - SIROS (solid line) and BSRN (dashed line) are shown for identical periods (~12 min) for three different days, April 18 (triangle), 15 (square), and 13 (circle). The resolution for both the instruments is degraded to 60 s. The error bars are ±5 W m^{-2}. Arrows represent approximate time during each day when a closure experiment was performed. The additional short-dashed line on April 18 represents ACR222 values which are well within the two NIP values.

to be represented by the degree of disagreement between the two NIPs, of 0.6%. If the fluctuations in the response of the instruments are uncorrelated, the combined uncertainty of a NIP measurement is

$$\Delta E_{\mathrm{NIP}} = \sqrt{0.3^2 + 0.6^2} = 0.67.$$

For both the ACR and the NIP, the large field of view of 5° and 5.7° (respectively) results in sampling of the atmospheric radiance in the solar aureole, a correction for which may be necessary, as described in section 4.5.

4.5. Corrections to Measurements of DNSI

The relatively large field of view of 5° and 5.7° in both ACR and NIP (respectively) results in sampling of energy in the solar aureole, the region in the immediate neighborhood of the Sun's disk. The aureole radiance is due mainly to atmospheric scattering of solar energy by particles large relative to visible wavelengths and is thus a function of particle loading. Aureole radiance is an undesirable quantity in a DNSI measurement and leads to an error in its measurement. Our estimate of this error is about 0.1% for the conditions encountered for the period of observations (details will be given in a future article). The estimate is based on a combination of MODTRAN 3 calculation and a narrow field-of-view (FOV) (1.2°) Sun photometer measurement of sky radiance in the solar aureole on a clear day. MODTRAN 3 calculation of sky radiance was accomplished by employing as input the measured AOT and radiosonde profiles of humidity and temperature and running it in the radiance mode with multiple scattering included. Computed sky radiance and the knowledge of the solar irradiance then were used to correctly predict the ratio of Sun photometer solar and sky response at three wavelengths of 441, 613, and 870 nm. An identical procedure this time with MODTRAN 3 run in the wavelength range 0.2-5 μm and applied to the much larger 5.7 FOV of the NIP yielded the ratio of energy contribution of the aureole to that of the Sun to be about 0.1%. Measured DNSI values will be reduced by 0.1% to account for this correction.

Atmospheric emittance in the 5° to 5.7° field of view of the

Table 4. Data and Results

Case	April 1996	Time UTC	Solar Zenith Angle, deg	Air Mass	AOT, 550 nm	Ångström Experiment	Path Water, cm	Measured DNSI (Corr) W m^{-2}	Model DNSI (Corr), W m^{-2}	Percent Difference*
1	13	14:34:05	59.686	1.98	0.12	0.7	2.22	786	778	-1.01
2	13	14:45:27	57.461	1.86	0.12	0.7	2.08	803	798	-0.70
3	13	17:30:28	30.426	1.16	0.10	0.8	1.37	959	946	-1.35
4	13	17:45:27	29.077	1.14	0.10	0.7	1.35	957	941	-1.72
5	15	14:59:55	54.120	1.71	0.06	1.6	1.31	920	914	-0.60
6	15	17:14:56	31.460	1.17	0.07	1.2	1.00	993	976	-1.73
7	15	17:29:57	29.780	1.15	0.08	1.2	0.98	1002	976	-2.67
8	15	17:44:57	28.400	1.14	0.08	1.2	0.97	994	977	-1.75
9	15	20:14:56	35.634	1.23	0.08	1.2	0.92	972	964	-0.86
10	18	14:12:36	62.659	2.18	0.10	0.6	2.37	778	773	-0.62
11	18	14:27:30	59.698	1.98	0.10	0.6	2.15	807	803	-0.58
12	18	14:34:04	58.398	1.91	0.09	0.6	2.07	819	816	-0.42
13	18	14:44:13	56.399	1.81	0.10	0.6	1.96	826†	826	0.01
14	18	17:14:17	30.544	1.16	0.08	0.7	0.77	978†	977	-0.08
15	18	17:29:16	28.822	1.14	0.08	0.7	0.75	974†	978	0.38
16	18	17:44:15	27.409	1.13	0.08	0.7	0.74	975†	985	1.02
17	19	17:14:04	30.247	1.16	0.08	0.7	1.28	953†	958	0.53
18	19	17:29:03	28.511	1.14	0.07	0.9	1.26	964†	973	0.92
19	19	17:44:03	27.083	1.12	0.08	0.7	1.25	968†	964	-0.39
20	19	23:25:24	70.483	2.99	0.12	0.5	2.75	639	642	0.44
21	19	23:35:06	72.424	3.31	0.12	0.5	3.05	593	596	0.53
22	19	23:37:12	72.484	3.32	0.13	0.5	3.06	577	580	0.49
23	20	14:25:03	59.696	1.98	0.08	1.0	1.71	829†	836	0.91
24	20	14:31:35	58.340	1.91	0.09	1.0	1.64	835†	842	0.91
25	20	14:43:47	55.990	1.79	0.08	1.0	1.54	853†	862	1.13
26	23	13:28:54	70.230	2.96	0.13	1.0	2.70	638	642	0.59
27	23	13:38:29	68.310	2.71	0.14	1.0	2.47	664	666	0.39
28	23	13:44:37	67.080	2.57	0.14	1.0	2.34	680	684	0.53
29	23	13:54:34	65.080	2.37	0.14	1.0	2.17	708	710	0.35
30	23	14:06:38	62.670	2.18	0.13	1.0	1.99	742	745	0.37
31	23	14:21:30	59.700	1.98	0.13	1.0	1.81	775	776	0.09
32	23	14:28:14	58.360	1.91	0.13	1.0	1.74	786	792	0.77
33	23	17:13:13	29.105	1.14	0.14	1.0	1.30	900†	903	0.32
34	23	17:28:14	27.305	1.13	0.16	1.0	1.28	905†	892	-1.45
35	23	17:43:16	25.820	1.11	0.16	1.0	1.27	907†	901	-0.66
36	23	17:58:17	24.709	1.10	0.15	1.0	1.25	911†	906	-0.58

All pertinent measurements and model-estimated DNSI are shown below for the 36 cases.
*calculated as (model-estimated DNSI - measured DNSI) as a percentage of modeled DNSI.
†ACR values.

detectors is a further potential source of error. In the presence of clouds, which are strong emitters of terrestrial thermal infrared energy, this correction could be a small but significant factor (~0.35% of DNSI). In the present study, the measurements are made in skies that are clear in the field of view of the sensors and under low PW conditions. The downward longwave flux is of the order of 300 W m^{-2} (as measured by a pyrgeometer) giving an atmospheric emittance contribution of ~0.7 W m^{-2}. This amount is subtracted (assumed constant) from the NIP and ACR measurements.

5. Results and Discussion

Radiosonde-measured temperature and RH as a function of pressure (and therefore height above ground level), Cimel Sun-photometer-measured AOT at 550 nm, and ozone from climatology are input to MODTRAN 3, which is run in the direct solar irradiance mode to compute DNSI. AOTs at wavelengths other than 550 nm were obtained by interpolation and extrapolation using the Ångström power law, after determining that such a power law fitted the Cimel measurements to within ±0.01. The radiosonde profiles are resampled at predetermined altitudes as required by the model (1 km apart in the lower levels and less frequently higher up), and for altitudes not probed by the radiosonde, the radiosonde profile is augmented by a standard midlatitude summer profile available in the model. Since it takes 5 minutes for the radiosonde to sample the boundary layer, where most of the water vapor is present, AOT, DNSI, and water vapor measurements taken within 15 minutes of the launch time were used. Data obtained at other times (that is more than 15 minutes from the radiosonde launch) were used only if it was concluded that the atmospheric properties were stable (the column-averaged properties were constant) between successive radiosonde launches. For a total of 6 days in April 1996, (April 13, 15, 18, 19, 20, and 23) NIP and ACR data were used as a measure of DNSI. Because of the lower uncertainty in ACR-measured DNSI values, the former are used whenever they are available.

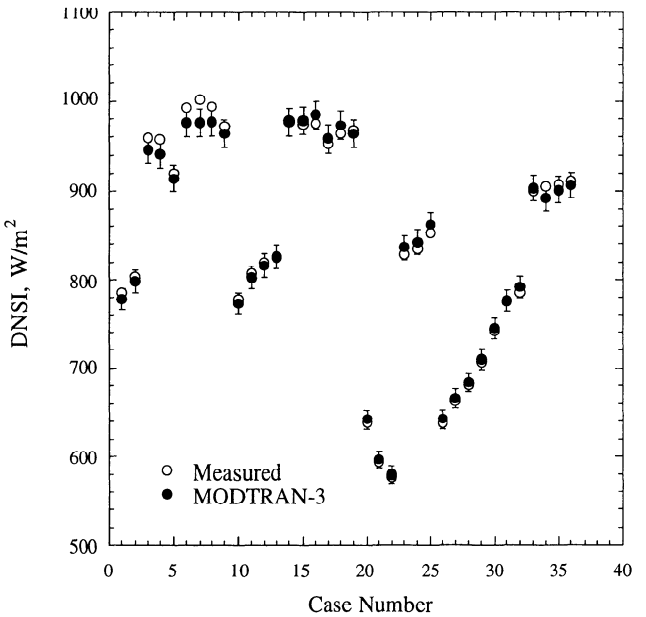

Figure 7. Model-estimated and NIP-measured DNSI are plotted versus case number, which represents the sequence of 36 cases between April 13 and 23, 1996 (Table 4). Error bars of ±1.6% represent the propagated uncertainty in the AOT measurement.

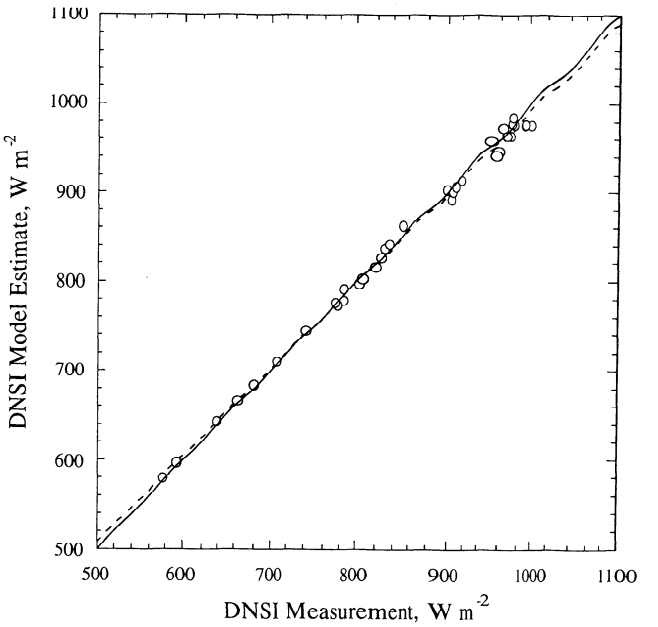

Figure 8. MODTRAN-3-estimated DNSI is plotted against NIP measured values; curve fit is shown by the dashed line. The 1:1 line (solid) is shown for comparison. The variation in DNSI is due mainly to variation in solar zenith angle. The correlation exhibits a bias (R^2=0.996). The linear fit to the data yields a slope of 0.97 and an offset of 22.9 W m^{-2}.

Thirty-six cases were identified as yielding instantaneous measurements of DNSI contemporaneously with radiosonde launches or otherwise satisfying requirement of atmospheric stability between launches. The quantities pertinent to the closure experiment are tabulated in Table 4. These include the data and time of the experiment, solar zenith angle and air mass, AOT at 550 nm and the fitted Ångström exponent used to determine AOT at wavelengths other than 550 nm, water column abundance along the path to the Sun, measured and modeled DNSI after applying all the corrections, and the percent difference between the measured and the model-estimated DNSI expressed as a percentage of model-estimated DNSI. Estimated and measured irradiance are plotted for comparison in Figures 7 and 8, with all the corrections, described previously, applied. No averaging is performed. In Figure 7, uncertainty bars on the model-calculated values of ±1.6% at air mass of 2 reflect mainly the uncertainty in AOT of 0.01, as deduced from the estimate of uncertainty in Cimel Sun photometer measurements for this period and the closeness of agreement with MFRSR values. In a Sun photometer measurement of AOT the uncertainty is inversely proportional to the air mass, being smaller for large angles [*Halthore et al.*, 1992a]. The uncertainty in DNSI estimate due to uncertainty in AOT is, however, proportional to the air mass. Thus to first order, these effects cancel each other, resulting in a constant uncertainty in the DNSI estimate as a function of air mass. Measurement uncertainty of ±5 W m^{-2}

for the NIP is too small (and for the ACR, even smaller) to be shown in Figures 7 and 8. Cases exhibiting low values of irradiance result from measurements at high solar zenith angles. Although the correlation between the model estimates and the measurements is excellent with an R^2 of 0.996 (Figure 8), on average the model slightly underestimates measured DNSI by (-0.18±0.94)%; for an average DNSI of 839 W m^{-2} this corresponds to -1.5 ±7.9 W m^{-2} (1 standard deviation) for the 36 measurements. The agreement between the model estimate and the measurement is well within the combined uncertainty estimate of 1.9% (obtained by combining uncertainty of 1.8% for the model estimate and 0.67% for the measurement, which are assumed to be uncorrelated), thus making this a successful closure experiment.

The dependence of the percent difference between model-estimated and measured DNSI on the air mass is examined (Figure 9) to infer possible inadequate accounting of atmospheric attenuation. If the attenuation (including absorption) in the model is not adequately accounted for, the percent difference will linearly increase with air mass. To analyze the trend, data above about 1.7 air mass (which shows less scatter than the rest) are fitted with a line that has a positive slope of 0.6 % air $mass^{-1}$. There also is significant scatter in these data consisting of 20 data points. The average unaccounted for attenuation (including absorption) of 0.38% corresponds to a vertical optical thickness of 0.0038. Is there a discernible trend in the percent difference with the amount of water vapor in the atmospheric path in the Sun's direction? A similar examination of the percent

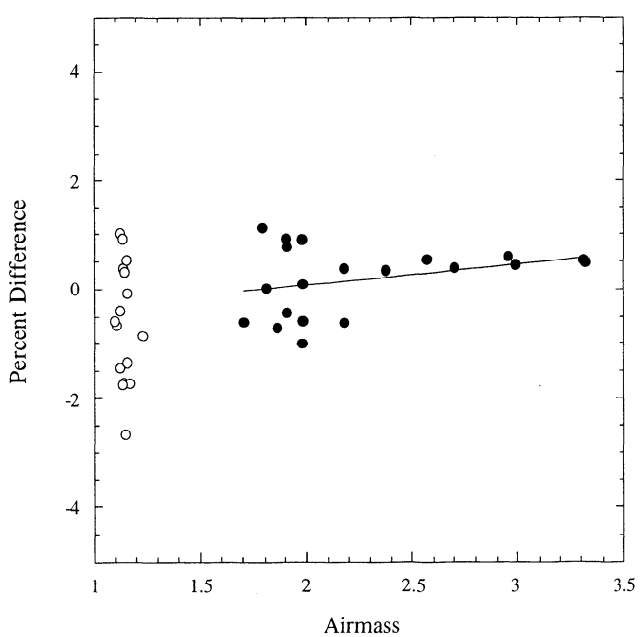

Figure 9. Percent difference, $(DNSI_{model} - DNSI_{meas})/DNSI_{model}$, between the model-estimated and the measured DNSI is plotted as a function of air mass to examine the effect of increasing column abundance of attenuators, especially gases. The spread in ordinate values at low air mass (open circles) is most likely due to atmospheric nonuniformity and atmospheric radiance effects in the FOV (see text). At large air mass (solid circles) defined as air mass greater than 1.7) slope of the linear fit is ~0.38%±0.27 air $mass^{-1}$.

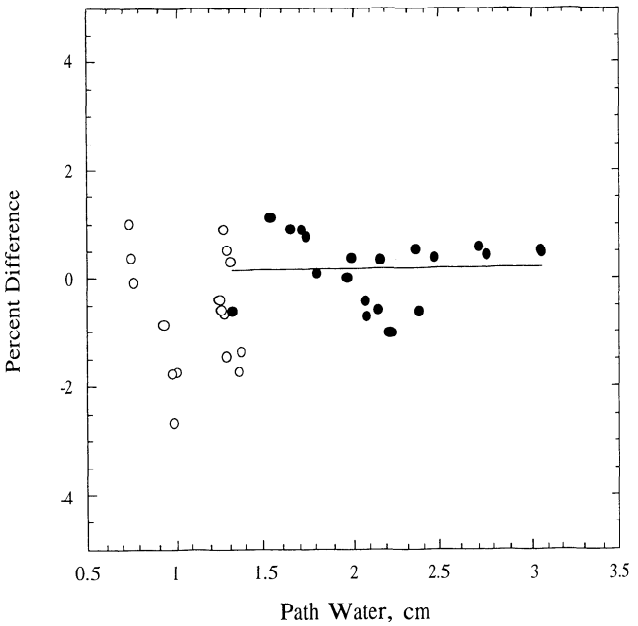

Figure 10. Percent difference, $(DNSI_{model} - DNSI_{meas})/DNSI_{model}$, between the model-estimated and the measured DNSI is plotted against the amount of water along the path. The slope of data points (solid circles corresponding to "high air mass" points in Figure 9) is 0.03% ±0.3 cm^{-1}. However, the linear fit is poor because of the scatter in the data.

difference as a function of path water abundance (Figure 10) shows that any trend is masked by a large relative scatter in the data points whose slope is 0.03% per cm H_2O. The unaccounted for absorption due to water vapor is therefore 3 X 10^{-2}%. Thus the lack of a significant trend in percent difference in Figures 9 and 10 shows that atmospheric attenuation, including absorption, is accurately accounted for in the model to within the stated uncertainties.

The variability in the percent difference between measured and model-estimated DNSI is greater at low air mass than at high air mass (Figure 9). This is probably due to uncorrelated fluctuations in NIP or ACR-measured DNSI and Cimel Sun photometer measured AOT. While the DNSI measurement by NIP or ACR is essentially instantaneous, tracking the increased fluctuations in DNSI at low air mass, the AOT measurement using Cimel Sun photometer (hence the MODTRAN 3 DNSI estimate) is an average of three measurements taken 30 s apart. Increased fluctuations in DNSI at or after local noon (low air mass) are due primarily to increased fluctuations in atmospheric transmittance, and in particular AOT (Table 2), and are attributed to increased convective activity induced by surface solar heating. Rising convective air parcels cause turbulent mixing of particles and moisture in the mixing layer, giving rise to the fluctuations in AOT by changing particle concentration and/or size. The diurnal effect on the AOT due to changes in mixing layer height has been discussed elsewhere [*Halthore et al.*, 1992b]. Changes in mixing layer height with maximum occurring an hour after local noon are observed in micropulse lidar images at the CART site [*Spinhirne et al.*, 1995]. An additional source of uncorrelated fluctuations between NIP or ACR-measured DNSI and Cimel Sun

photometer measured AOT could be the difference in fields of view between the two sensors (5.7° and 1.2°, respectively).

Result presented in Figure (9) allows us to establish a limit on the atmospheric absorption that is unaccounted for in MODTRAN 3 in irradiance units. Linear fit of the difference between model estimated and measured DNSI plotted as a function of air mass (Figure 9) for air mass greater than 1.7 with a slope of 0.38% per air mass, translates to an unaccounted for absorption of about 6 ±4 W m^{-2}. This follows from the assumption of dayside average total downward and upward irradiance through the lower part of the atmosphere of 800 W m^{-2}, dayside average solar zenith angle of 60°, yielding an average unaccounted for absorption of about $((0.38\pm0.27) / 100) \times 2 \times 800 \approx 6 \pm 4$ W m^{-2}. In contrast, *Arking* [1996] found, on the basis of analysis of a global radiation data set that a general circulation model (GCM), representative of many GCMs currently in use, underestimated the globally averaged solar flux absorbed in the atmosphere by 25 to 30 W m^{-2}, which corresponds to 50 to 60 W m^{-2} in the instantaneous flux for a dayside average solar zenith angle of 60° or ~0.025 in vertical optical thickness (compare with 0.0038, the average unaccounted for attenuation).The discrepancy was attributed by Arking principally to inadequate parameterization of absorption by water vapor or other components, such as aerosols, which spectrally correlate with water vapor. If MODTRAN 3 suffered the same inadequacies in parameterization, the resulting effect on DNSI would be readily apparent as a bias that would increase with increasing air mass (slope ~ 2.5% air $mass^{-1}$) or water path abundance. Clearly, this is inconsistent with the present finding. Thus the MODTRAN 3 calculation of DNSI, and by extension its treatment of atmospheric absorption, does not appear to exhibit the underestimated absorption that Arking ascribed to GCMs.

6. Conclusions

Comparison of the measured and model-estimated direct normal solar irradiance constitutes a simple yet robust closure experiment. The simplicity arises from the need to know only the extinction properties of the atmosphere without regard to scattering properties. The robustness arises from the relatively low uncertainties in the measurement of DNSI and other atmospheric quantities that are used in the prediction of DNSI. A medium-resolution radiative transfer program, MODTRAN 3, which uses band models for atmospheric absorption which represent current knowledge of absorption by atmospheric gases in the solar spectrum, together with measured values of AOT, water vapor and ozone, was used to estimate DNSI. DNSI and the atmospheric variables required as model inputs were measured, with quantified uncertainties, at a highly instrumented site in north central Oklahoma. For 36 independent measurements the model slightly underestimated the measured DNSI by (-0.18 ±0.94)% (1 standard deviation). This degree of disagreement is well within the combined uncertainties of model calculation (1.8%) and DNSI measurement (0.3% for ACR and 0.67% for NIP). The data-base on which MODTRAN 3 band model parameters are based is therefore suitable for incorporation into global and climate and weather models, either directly or as the basis for subsequent parametrization as may be required by particular models. The uncertainty in the model calculation of 1.8% is dominated by the effect (1.6%) of uncertainty in AOT measurement of 0.01 at air mass of 1. In view of the diverse nature of measurements that are employed in this rather simple closure experiment, the disagreement is surprisingly small. The bias (-0.18%) and the standard deviation (0.94%) of the difference between model calculation and the measurement could be due to an unknown combination of factors that may include the solar constant used in the model which contributes the maximum correction to the DNSI measurement and the uncertainty in the AOT measurement, which is the main contributor to the uncertainty in model calculation of DNSI. Possible future directions for experiments of this sort involve reducing the error in the knowledge of the extraterrestrial solar spectral irradiance and better characterization of the AOT in the solar spectrum, but especially in the 1-5 μm range.

Appendix

ACR	absolute cavity radiometer
AOT	aerosol optical thickness
ARM	atmospheric radiation measurement
BNL	brookhaven national laboratory
CART	cloud and radiation test bed
CF	central facility
DNSI	direct-normal solar irradiance
DNSSI	direct-normal spectral solar irradiance
DOE	department of energy
ERBS	earth radiation budget satellite
FASCODE	fast atmospheric signature code
FASE	fascode for environment
HITRAN	a molecular spectroscopic database
IOP	intensive operations period
IR	infrared
LOWTRAN	low-resolution radiative transfer code (20 cm^{-1} resolution).
MFRSR	multifilter rotating shadow-band radiometer
MODTRAN	moderate resolution lowtran code (2 cm^{-1} resolution)
NIP	normal incidence pyrheliometer
NOAA	national oceanic and atmospheric administration
PW	precipitable water, cm
RH	relative humidity
SGP	southern great plains (north central oklahoma)
SIROS	solar and infrared observation station
SMM	solar maximum mission (satellite)
TIROS-N	television and infrared observation satellite, NOAA
TOVS	TIROS n operational vertical sounder
UARS	upper atmospheric research satellite
UT	universal time
WRR	world radiation reference

Acknowledgments. CART site data were obtained from the ARM program sponsored by the U.S. Department of Energy (DOE). Absolute Cavity Radiometer DNSI data were obtained from M. Rubes and J. DeLuisi (NOAA). Arthur Neuendorffer (NOAA) provided the TOVS total ozone data for the CART site. Cimel Sun photometer data are obtained from the AERONET network managed by one of the

authors (BH). The FASE calculations were done by Hilary E. Snell of Atmospheric and Enviromental Research, Inc., under AF contract F19628-93-C-0040, partially funded by the AF and DOE/PNL ARM subcontract 218101-A-Q1 to Phillips Laboratory. MODTRAN was developed with Alex Berk, Lawrence S. Bernstein, and Prabhat K. Acharya, all of Spectral Sciences, Inc., under AF contracts F19628-93-C-0049 and F1962891-C-0083. At ECN, grants partly from the Climatology and Natural Hazards Programme of the EC-ENVIRONMENT Programme (contract no. EV5V-CT92-0171), from the National Research Program on Climate Change (contract 951205), and from the Ministry of Economic Affairs of the Netherlands (Mefis 53478) are acknowledged. Dan Imre, Brookhaven National Labratory, and Chris Gueymard, Florida Solar Energy Center, are acknowledged for helpful comments in the course of this work, and Arjan Hensen, ECN, is acknowledged for critical comments on the manuscript.

References

Anderson, G. P, et al., MODTRAN 3: Suitability as a flux-divergence code, in *Proceedings of the 4th ARM Science Team Meeting* (1994), *DOE Rep. CONF-940277*, U. S. Dep. of Energy, Washington, D. C., pp. 75-80, 1995.

Arking, A., Absorption of solar energy in the atmosphere: discrepancy between model and observations, *Science, 273*, 779-782, 1996.

Bruegge, C. J., R. N. Halthore, B. L. Markham, M. Spanner, and R. Wrigley, Aerosol optical depth retrievals over the Konza Prairie, *J. Geophys. Res., 97*, 18,743-18,758, 1992.

Cess, R. D., et al., Absorption of solar radiation by clouds: Observations versus models, *Science, 267*, 496-499, 1995.

Clough, S.A., Radiative transfer model development in support of the Atmospheric Radiation Measurement (ARM) Program, in *Proceedings of the 2nd ARM Science Team Meeting* (1991), *DOE Rep. CONF-9110336*, pp. 21-24, U. S. Dept. of Energy, Washington, D. C., 1992.

Halthore, R. N., and B. L. Markham, Overview of atmospheric correction and radiometric calibration efforts during FIFE, *J. Geophys. Res., 97*, 18,731-18742, 1992a.

Halthore, R. N., B. L. Markham, R. A. Ferrare, and T. O. Aro, Aerosol optical properties over the mid-continental United States, *J. Geophys. Res., 97*, 18,769-18778, 1992b.

Halthore, R. N., T. F. Eck, B. N. Holben, and B. L. Markham, Sun photometric measurements of atmospheric water vapor column abundance in the 940-nm band, *J. Geophys. Res., 102*, 4343-4352, 1997.

Harrison, L., J. Michalsky, and J. Berndt, Automatic multifilter rotating shadow-band radiometer: An instrument for optical depth and radiation measurements, *Appl. Opt., 33*, 5118-5125, 1994.

Imre, D. G., E. H. Abramson, and P. H. Daum, Quantifying cloud-induced shortwave adsorption: An examination of uncertainties and of recent arguments for large excess absorption, *J. Appl. Meteorol., 35*, 1991-2010, 1996.

Kurucz, R. L., The solar irradiance by computation, in *Proceedings of the 17th Annual Review Conference on Atmospheric Transmission Models*, edited by G. P. Anderson, R. H. Picard, and J. H. Chetwynd, 332pp., Phillips Lab., Geophys. Dir., Bedford, Mass., 1995.

Lean, J., Variations in the Sun's radiative output, *Rev. Geophys., 29*, 505-535, 1991.

Lesht, B. M., and J. C. Liljegren, Comparison of precipitable water vapor measurements obtained by microwave radiometry and radiosondes at the Southern Great Plains CART site, in *Proceedings of the 5th ARM Science Team Meeting* (1996), DOE Rep., U. S. Dep. of Energy, Washington, D. C., in press, 1997.

Markham, B. L., and J. L. Barker, Thematic Mapper bandpass solar exo-atmospheric irradiances, *Int. J. Remote Sens., 8*, 517-523, 1987.

Michalsky, J., J. C. Liljegren, and L. C. Harrison, A comparison of Sun photometer derivations of total column water vapor and ozone to standard measures of same at the southern Great Plains Atmospheric Radiation Measurement site, *J. Geophys. Res., 100*, 25,995-26,003, 1995.

Michalsky, J., M. Rubes, T. Stoffel, M. Wesely, M. Splitt, and J. DeLuisi, Optimal measurement of surface shortwave irradiance using current instrumentation - The ARM experience, in *Proceedings of the Ninth Conference on Atmospheric Radiation*, pp. J5-J9, *Am. Meteorol. Soc.*, Boston, Mass., 1997.

Neckel, H., and D. Labs, The solar radiation between 3300 and 12,500 A, *Sol. Phys., 90*, 205-258, 1984.

Neuendorffer, A., Ozone monitoring with TIROS N operational vertical sounders, *J. Geophys. Res., 101*, 18,807-18,828, 1996.

Penner, J. E., R. J. Charlson, J. M. Hales, N. S. Laulainen, R. Leifer, T. Novakov, J. Ogren, L. F. Radke, S. E. Schwartz, and L. Travis, Quantifying and minimizing uncertainty of climate forcing by anthropogenic aerosols, *Bull. Am. Meteorol. Soc., 75*, 375-400, 1994.

Pilewskie, P., and F. P. J. Valero, Direct observations of excess solar absorption by clouds, *Science, 257*, 1626-1629, 1995.

Quinn, P. K., T. L. Anderson, T. S. Bates, R. Dlugi, J. Heintzenberg, W. von Hoyningen-Heune, M. Kulmala, P. B. Russell, and E. Swietlicki, Closure in tropospheric aerosol-climate research: A review and future needs for addressing aerosol direct shortwave radiative forcing, *Beitr. Phys. Atmos., 69*, 547-577, 1996.

Ramanathan, V., B. Subasilar, G. J. Zhang, W. Conant, R. D. Cess, J. T. Kiehl, H. Grassl, and L. Shi, Warm pool heat budget and shortwave cloud forcing: A missing physics?, *Science, 267*, 499-503, 1995.

Reagan, J. A., P. A. Pilewskie, I. C. Scott-Fleming, B. M. Herman, and A. Ben-David, Extrapolation of earth-based solar irradiative measurements to exoatmospheric levels for broad-band and selected absorption-band observations, IEEE Trans. Geosci. REmote Sens., GE-25 (6), 647-653, 1987.

Romero, J., N. P. Fox, and C. Frohlich, Improved comparison of the World Radiometric Reference and the SI radiometric scale, *Metrologia, 32*, 523-524, 1995/1996.

Shaw, G. E., Sun photometry, *Bull. Am. Meteorol. Soc., 64*, 4-10, 1983.

Shettle, E. P., and S. M. Anderson, New visible and near ir ozone absorption cross-sections for MODTRAN, in *Proceedings of the 17th Annual Conference on Atmospheric Transmission Models*, edited by G. P. Anderson, R. H. Picard, and J. H. Chetwynd, pp. 335-345, PL-TR-95-2060, Phillips Lab/Geophysics directorate, Bedford, Mass., 1995.

Snell, H. E., W. O. Gallery, D. B. Hogan, J. L. Moncet, G. P. Anderson, J. H. Chewynd, S. Miller, and J. Wang, FASCODE for the Environment (FASE), in *Proceedings of the 6th ARM Science Team Meeting, DOE Rep.*, U. S. Dep. of Energy, Washington, D. C., June 1997.

Spinhirne, J. D., J. A. R. Rall, and V. S. Scott, Compact eye safe lidar systems, *Rev. Laser Eng., 23*, 112-118, 1995.

Stephens, G. L., How much solar radiation do clouds absorb?, *Science, 271*, 1131-1133, 1996.

Stokes, G. M., and S. E. Schwartz, The Atmospheric Radiation Measurement (ARM) Program: Programmatic background and design of the cloud and radiation test bed, *Bull. Am. Meteorol. Soc., 75*, 1201-1221, 1994.

Wiscombe, W. J., An absorbing mystery, *Nature, 376*, 466-467, 1995.

R. N. Halthore and S. E. Schwartz, Department of Applied Science, Brookhaven National Laboratory, Upton, NY 11973-5000. (e-mail: halthorc@bnl.gov; ses@bnl.gov)

J. J. Michalsky, Atmospheric Sciences Research Center, State University of New York at Albany, Albany, NY. (e-mail: joe@asrc.cestm.albany.edu)

G. P. Anderson, Phillips Laboratory/Geophysics Directorate, Hanscom Air Force Base, MA. (e-mail: ganderson@PLH.AF.MIL)

R. A. Ferrare, Hughes STX Corporation, Lanham, MD. (e-mail: rferrare@larc.nasa.gov)

B. N. Holben, NASA Goddard Space Flight Center, Greenbelt, MD. (e-mail: brent@ spawer.gsfc.nasa.gov)

H. M. Ten Brink, Netherlands Energy Research Foundation, ECN, Petten, Netherlands.

(Received April 16, 1997; revised August 26,1997;
accepted September 11, 1997.)